Supporting Information for:

Directing the Outcome of CO_2 Reduction at Bismuth Cathodes Using Varied Ionic Liquid Promoters

Abderrahman Atifi,‡ David W. Boyce,‡ John L. DiMeglio,‡ and Joel Rosenthal*

Department of Chemistry and Biochemistry, University of Delaware, Newark, DE 19716

Corresponding author: joelr@udel.edu

Index

Experimental Methods

Experimental Methods

General. Reagents and solvents were purchased from Sigma-Aldrich, Acros Organics, Fisher, Alfa Aesar, TCI America, Matrix Scientific, or Cambridge Isotopes Laboratories. Bismuth(III) nitrate pentahydrate (99.999%), and 1-n-Butyl-3-methylimidazolium hexafluorophosphate (98+%) were purchased from Alfa Aesar. 1,8-Diazabicyclo[5.4.0]undec-7ene, 98% (DBU) was purchased from Acros Organics. Ammonium hexafluorophosphate (99+%) was purchased from Matrix Scientific. Electrochemical grade tetrabutylammonium hexafluorophosphate ($TBAPF_6$) was purchased from TCI America and purified by recrystallization from ethanol. Carbon dioxide was purchased from Keen Compressed Gas Company. DBU was dried over activated molecular sieves prior to use, while all other chemicals were used without further purification. Bismuth-modified cathode materials were prepared via electrodeposition as previously reported.[1] [DBU–Et]Br was prepared using a previously described method.[2]

Physical Methods. ^{1}H, ^{13}C, and ^{19}F NMR were recorded at 25 °C on a Bruker 600 MHz spectrometer. High-resolution mass spectrometry analyses were performed by the Mass Spectrometry Laboratory in the Department of Chemistry and Biochemistry at the University of Delaware.

Electrochemical Measurements. All electrochemistry was performed using either a CHI-620D potentiostat/galvanostat or a CHI-720D bipotentiostat. Cyclic voltammetry and linear-sweep voltammetry experiments were performed using standard three-electrode configurations. The working electrodes were either a bare glassy carbon disk electrode (GCE, 3.0 mm diameter CH Instruments) or a Bi-modified electrode. Platinum gauze or wire (Sigma, 99.9%) was used as the counter electrode. All potentials were recorded versus a Ag/AgCl reference electrode (1.0 M KCl, CH Instruments) and converted to the SCE reference scale ($E_{SCE} = E_{Ag/AgCl} + 0.044$ V). Unless otherwise indicated, 0.1 M $TBAPF_6$ was used as supporting electrolyte, and voltammograms were recorded at 100 mV/s with iR drop compensation.

Electrodeposition of Bi-modified electrodes. A glassy carbon disk electrode (GCE, 3.0 mm diameter) or glassy carbon plate (1 cm × 3 cm) was polished with a slurry of 0.05 micron alumina powder in Millipore water. Residual alumina was rinsed from the GCE surface with Millipore water, and the electrode was then sonicated in Millipore water for five minutes. The polished GCE was placed in an electrodeposition bath containing 20 mM bismuth(III) nitrate, 1.0 M hydrochloric acid and 0.5 M KBr. The GCE was preconditioned by cycling the applied potential (10 cycles) from 0 to –0.55 V vs. SCE at a sweep rate of 100 mV/sec and was then briskly agitated in the deposition solution to remove any exfoliated material from the GCE surface. Controlled potential electrolysis (CPE) was initiated using this conditioned GCE in the quiescent Bi^{3+} solution at –0.21 V versus SCE until ~3 C/cm^2 of charge had been passed. The bismuth-modified GCE was sequentially rinsed with 1 M hydrochloric acid, Millipore water, and acetonitrile prior to being dried under a gentle stream of nitrogen. As demonstrated in a prior study,[1] the roughness factor of the Bi-modified GCE was determined to be 1.3.

Computations. All density functional calculations were performed with the Gaussian 09 (G09) program package[3], using the m062X density functional[4] with the 6-311+G(d,p) basis

set. The calculations in acetonitrile used the SMD universal continuum model[5] with ε =35.688. All geometry optimizations were performed in C1 symmetry with subsequent frequency analysis to confirm that each stationary point was a minimum on the potential energy surface.

CO_2 Reduction Electrolysis and Product Analysis. Current densities were determined by performing controlled potential electrolyses (CPE) in gas-tight two-compartment cells with a Nafion (NRE-212) membrane separating the anode and cathode compartments (schematic illustration of cell is shown in Figure S5). In all experiments both the anode and cathode compartments contained a total volume of 20 mL solvent and were sparged with either CO_2, Ar or N_2 for at least 30 minutes prior to performing experiments.

During all CPE experiments, the cathode solution was stirred vigorously while a constant supply of CO_2 gas was delivered to the headspace of the cell at a rate of 5.0 cm^3/min. The cathode compartment was vented directly into the sampling loop of a gas chromatograph (GC) (SRI Instruments, SRI-8610C). A GC acquisition was initiated in 15 min increments by placing the sampling loop in line with both a packed HayeSep D column and a packed MoleSieve 13X column. Argon (Keen, 99.999%) was used as the GC carrier gas. The GC columns led directly to a thermal conductivity detector (TCD) to quantify hydrogen and a flame ionization detector (FID) equipped with a methanizer to quantify carbon monoxide. The partial current densities associated with production of CO and H_2 were calculated from the GC peak area as follows:

$$j_{\mathrm{CO}} = \frac{\text{Peak Area}}{\alpha} \times \text{Flow Rate} \times \frac{2\mathrm{Fp}_0}{\mathrm{RT}} \times (\text{Electrode Area})^{-1}$$

$$j_{\mathrm{H_2}} = \frac{\text{Peak Area}}{\beta} \times \text{Flow Rate} \times \frac{2\mathrm{Fp}_0}{\mathrm{RT}} \times (\text{Electrode Area})^{-1}$$

where α and β are the conversion factors based on calibration of the GC with standard samples of CO and H_2, respectively, F = 9.65 x 10^4 C mol^{-1}, p_0 = 1 atm, R = 82.1 mL atm K^{-1} mol^{-1}, and T = 298 K. Faradaic efficiencies for a given product were calculated by dividing these partial current densities by the total current density.

Formate ($HCOO^-$) production was quantified post-electrolysis by ^{1}H NMR spectroscopy. Standards with known concentrations of formic acid were prepared in acetonitrile (MeCN) containing a known concentration (1.0 mM) of CH_2Cl_2, as an internal reference. In a typical sample, the NMR tube contained 0.5 mL of the formic acid standard, 0.1 mL of deuterated MeCN, 0.02 mL of a 31 mM solution of CH_2Cl_2 in MeCN and 0.02 mL of D_2O. Using the solvent suppression method described below, the integration of the formate proton peak area was accomplished by normalizing the peak area of the internal CH_2Cl_2 reference to two protons. Plotting the peak areas versus formic acid concentrations of the standards gives an experimental slope of unity.

The amount of formic acid produced during a bulk electrolysis experiment was determined in a manner similar to that employed for the calibration experiment (vide supra). A 0.5 mL sample of the catholyte solution was mixed with 0.1 mL CD_3CN, 0.02 mL D_2O, and 0.02 mL of a 31 mM solution of CH_2Cl_2 in MeCN. Spectra were locked onto CD_3CN and D_2O

was used to mask the large signals associated with $[DBU–H]^+$. Using the experimental calibration slope, the number of moles of formic acid was determined based on the molarity (1 mM) of the internal CH_2Cl_2 reference. In this way, a straight reading of the integrated area of the formate peak (8.61 ppm) gives the concentration of the formic acid in the NMR tube in mM, which is then corrected to the actual concentration in the catholyte compartment (20 mL). A typical ^1H NMR spectrum obtained using the above protocol is shown in Figure S8.

All ^1H NMR spectra for formate were acquired using a pre-saturation technique to suppress the large CH_3CN signal. The pre-saturation pulse program[6] for signal suppression with the saturation pulse frequency was centered at the resonance of the methyl group of the MeCN solvent (1.96 ppm). Since the methyl signal is sufficiently far away from the formate signal (8.61 ppm), the pre-saturation pulse program is able to produce quantitative results. Considering the slow proton relaxation of the formate proton, a carefully calibrated 90-degree pulse with a long relaxation delay (5 seconds) was used throughout the NMR experiment.

Estimation of the CO_2 to $HCOO^–$ standard reduction potential in MeCN. The standard reduction potential (E°) for the conversion of CO_2 to $HCOO^–$ (FA) has not been determined for the acetonitrile-based catholytes used herein. According to the thermodynamic cycle in Scheme S1, the equation below allows for the determination of the free energy associated with $HCOO^–$ production.

Scheme S1. Thermodynamic cycle used to determine the free energy change associated with CO_2 reduction to $HCOO^–$

$$C_{(s)} + O_{2(g)} + H_{2(g)} \rightleftharpoons HCOOH_{(l)} \qquad \Delta G_f(FAH) = -361.4 \text{ kJ/mol}$$

$$HCOOH_{(l)} \rightleftharpoons HCOOH_{(g)} \qquad \Delta G_{vap}(FAH) = 4.35 \text{ kJ/mol}$$

$$HCOOH_{(g)} \rightleftharpoons HCOOH_{(MeCN)} \qquad \Delta G_{sol}(FAH) = -23.0 \text{ kJ/mol}$$

$$HCOOH_{(MeCN)} \rightleftharpoons HCOO^-_{(MeCN)} + H^+_{(MeCN)} \qquad \Delta G_{K_a}(FAH) = 110.1 \text{ kJ/mol}$$

$$H^+_{(MeCN)} + e^-_{(Fc^{+/0})} \rightleftharpoons 1/2\ H_{2(g)} \qquad \Delta G_{HER} = 2.7 \text{ kJ/mol}$$

$$C_{(s)} + O_{2(g)} \rightleftharpoons CO_{2(g)} \qquad \Delta G_f(CO_2) = -394.39 \text{ kJ/mol}$$

$$CO_{2(g)} + H^+_{(MeCN)} + 2e^-_{(Fc^{+/0})} \rightleftharpoons HCOO^-_{(MeCN)} \qquad \Delta G_{CO_2/FA} = -129.84 \text{ kJ/mol}$$

$$\Delta G_{CO_2/FA} = \Delta G_f(FAH) + \Delta G_{vap}(FAH) + \Delta G_{sol}(FAH) + \Delta G_{Ka}(FAH) + 2\Delta G_{HER} - \Delta G_f(CO_2)$$

A similar approach has been used for the determination of E^o for the reduction of CO_2 to CO in organic solutions.[7–9] The free energy change associated with the formation of formic

acid (ΔG_f(FAH)), the vaporization of formic acid (ΔG_{vap}(FAH)), and the formation of CO_2 ($\Delta G_f(CO_2)$) are known values.[10,11] The free energy associated with hydrogen evolution (ΔG_{HER}) was determined from the reported H^+/H_2 potential in acetonitrile using $\Delta G = nFE^o$.[12] The free energy change during formic acid dissolution (ΔG_{sol}(FAH)) and deprotonation (ΔG_{Ka}(FAH)) are calculated in this work. Using these thermodynamic values, the Gibbs energy associated with the reduction of CO_2 to FA ($\Delta G_{CO_2/FA}$) is determined to be –128.84 kJ/mol.

$$\Delta G_{CO_2/FA} = -129.84 \text{ kJ/mol}$$

Using the relationship $\Delta G = -nFE^o$, the standard reduction potential for the $CO_2/HCOO^-$ couple in acetonitrile is determined to be –0.673 V vs. $Fc^{(+/o)}$. The calculated potential is referenced to the ferrocene/ferrocenium ($Fc^{(+/0)}$) couple, as the hydrogen evolution potential in acetonitrile was measured against this reference. The formal potential for the ferrocene$^{(+/0)}$ couple has been reported as 0.4 V vs. SCE for MeCN solutions of $TBAPF_6$, similar to those used in this work.[13,14] Using the conversion E (V vs. $Fc^{(+/0)}$) + 0.4 = E (V vs. SCE), we obtain a value of –0.273 V vs. SCE for the reduction of CO_2 to $HCOO^-$ in acetonitrile solutions.

$$E^o_{CO_2/FA,\ MeCN} = -\frac{\Delta G_{CO_2/FA}}{2F} = -0.673 \text{ V vs. } Fc^{+/0} = -0.273 \text{ V vs. SCE}$$

The equilibrium potential for CO_2 reduction to $HCOO^-$ under the conditions used in this paper is approximated by the equations below.

$$E^{eq}_{CO_2/FA} = -0.273 - \frac{RT\ln(10)}{2F}\ pK_a([DBU\text{–}H]^+, MeCN)$$

$pK_a([DBU\text{–}H]^+, MeCN)$ = 24.3,[15] which leads to $E^{eq}_{CO_2/FA} = -0.90$ V vs. SCE

Estimation of the CO_2 to HCOOH Standard Reduction Potential in MeCN. Cathodic polarization of a Bi-modified electrode predominantly yields $HCOO^-$ as determined by ^1H NMR spectroscopy. Instead of the $2e^-/1H^+$ reduction of CO_2 to yield $HCOO^-$ directly, an alterative mechanism is the $2e^-/2H^+$ reduction of CO_2 to yield HCOOH, followed by deprotonation. As we cannot rule out this potential mechanism, the $\Delta G_{CO_2/FAH}$ and $E^o_{CO_2/FAH,\ MeCN}$ were determined using the thermodynamic cycle shown in Scheme S2.

Scheme S2. Thermodynamic cycle used to determine the free energy change associated with CO_2 reduction to HCOOH

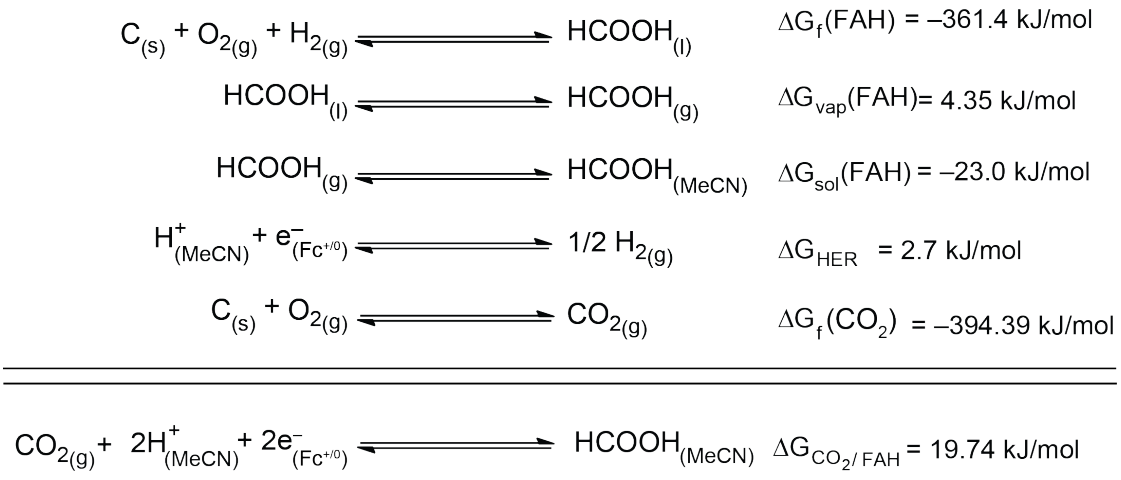

$$\Delta G_{CO_2/FAH} = \Delta G_f(FAH) + \Delta G_{vap}(FAH) + \Delta G_{sol}(FAH) + 2\Delta G_{HER} - \Delta G_f(CO_2)$$

$$\Delta G_{CO_2/FAH} = 19.74\ \text{kJ/mol}$$

$$E^{o}_{CO_2/FAH,\ MeCN} = -\frac{\Delta G_{CO_2/FAH}}{2F} = -0.102\ \text{V vs. Fc}^{+/0} = 0.298\ \text{V vs. SCE}$$

The equilibrium potential for CO_2 reduction to HCOOH under the conditions used in this paper is approximated by the equations below.

$$E^{eq}_{CO_2/FAH} = 0.298 - \frac{RT\ln(10)}{F}\ pK_a([DBU\text{–}H]^+, MeCN)$$

$pK_a([DBU\text{–}H]^+, MeCN)$ = 24.3, which leads to $E^{eq}_{CO_2/FAH} = -1.14$ V vs. SCE

Calculated Solvation Free Energy of Formic Acid in Acetonitrile. The solvation free energy of formic acid in acetonitrile (ΔG_{sol}(FAH)) was determined by G09 calculations on geometry-optimized formic acid in the gas phase and solvated in MeCN. ΔG_{sol}(FAH) was determined to be –23.0 kJ/mol from the difference of the free energy of MeCN solvated formic acid ($G_{FAH,\,s}$) and formic acid in the gas phase ($G_{FAH,\,g}$).

Calculated pK_a of HCOOH in MeCN. The thermodynamic cycle in Scheme S1 requires knowledge of the acid dissociation constant (K_a) of HCOOH in MeCN to calculate the free energy associated with deprotonation (ΔG_{Ka}(FAH)). To the best of our knowledge, the pK_a of HCOOH in MeCN is not reported. Accordingly. We sought to calculate this pK_a using the direct method, involving the thermodynamic cycle in scheme S3.[16]

Scheme S3. Thermodynamic cycle for the direct calculation of pK_a,

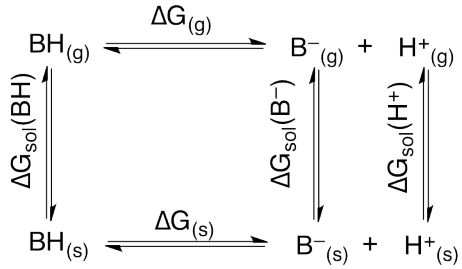

Using this general scheme the pK_a for a variety of known acids were calculated using the following equations. Subscript (s) designates solvation in MeCN.

$$\Delta G_{(g)} = G_{H^+(g)} + G_{B^-(g)} - G_{BH(g)}$$

$$\Delta G_{(S)} = \Delta G_{(g)} + \Delta G_{sol}(H^+) + \Delta G_{sol}(B^-) - \Delta G_{sol}(BH)$$

$$pK_a(BH) = -\log K_a = \frac{\Delta G_{(s)}}{\ln(10)\,RT}$$

G_{H+} = –6.28 kcal/mol[17]

$\Delta G_{sol}(H^+)$ =–258.3 kcal/mol[18,19]

The remaining gas phase free energies and solvation energies were calculated using G09 on a series of standard acids (BH) and conjugate bases (B^-). These calculated pK_a values are displayed against their literature values in the plot on the following page and in Table S1.[20]

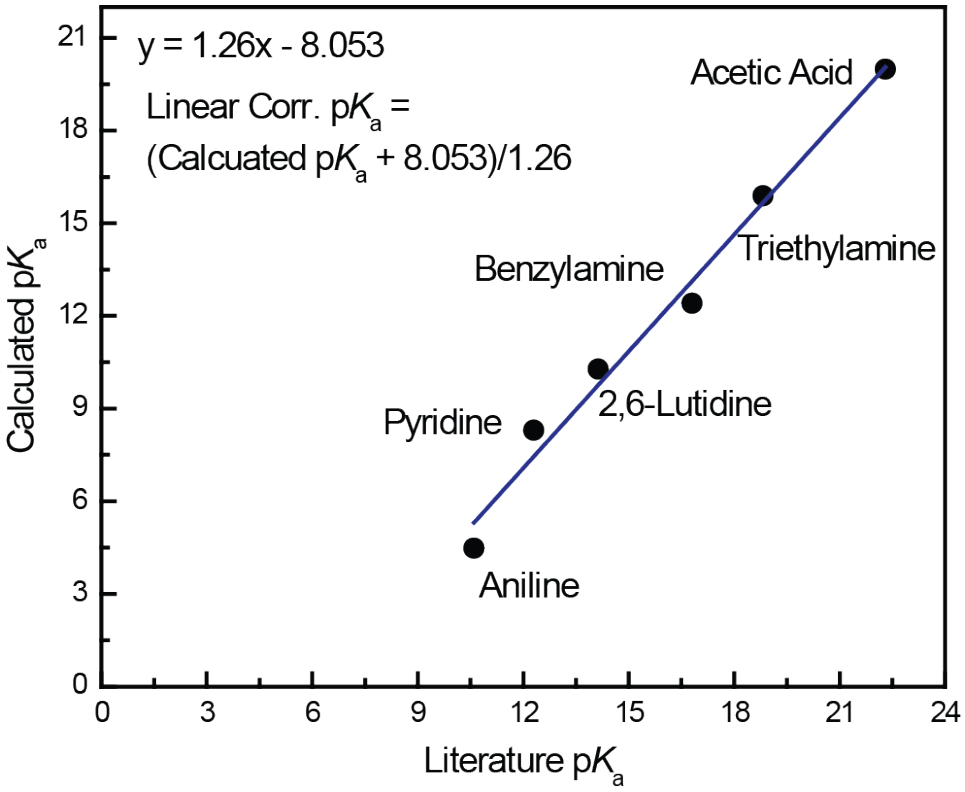

As shown by the above plot, the directly calculated pK_a values deviate by up to 6 pK_a units from literature values. This error, however, is systematic as evidenced by the linear correlation between calculated and literature pK_a. Previous studies have improved the accuracy of direct pK_a calculations by applying a linear correction that forces the pK_a data to have a slope of 1 and an intercept of zero.[21,22] As shown in Table S1, application of this linear correction significantly reduces the maximum pK_a deviation to < 0.7 pKa units. Using this method, the pK_a of HCOOH in MeCN was determined to be 19.6.

Table S1. Comparison of literature MeCN pK_a values of several standard acids and bases with those calculated using DFT and those from linear correction of the DFT values.

	Literature pK_a	Calculated pK_a	Linear Corr. pK_a
Aniline	10.6	4.48	9.95
Pyridine	12.3	8.30	12.98
2,6-Lutidine	14.13	10.28	14.55
Benzylamine	16.8	12.41	16.24
Triethylamine	18.82	15.89	19.00
Acetic Acid	22.3	19.99	22.26
Formic Acid	N/A	16.69	19.64

The calculated pK_a of HCOOH using the direct method was compared to values obtained using an isodesmic scheme (Scheme S4). In this cycle, the deprotonation of formic acid is coupled with the protonation of acetate (OAc) to give acetic acid (AcOH). Unlike in the direct method, an experimental value for $\Delta G_{sol}(H^+)$ is no longer needed, yielding a more reliable pK_a calculation.

Scheme S4. Isodesmic thermodynamic cycle used to determine the pK_a of HCOOH in MeCN

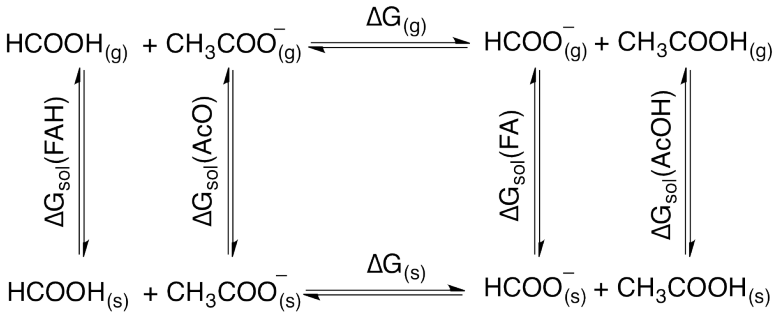

$$\Delta G_{(g)} = G_{FA(g)} + G_{AcOH(g)} - G_{AcO(g)} - G_{FAH(g)}$$

$$\Delta G_{(S)} = \Delta G_{(g)} + \Delta G_{sol}(FA) + \Delta G_{sol}(AcOH) - \Delta G_{sol}(AcO) - \Delta G_{sol}(FAH)$$

$$pK_a(HCOOH) = \frac{\Delta G_{(s)}}{\ln(10)\,RT} + pK_a(AcOH) = 19.0$$

Using scheme S4, the pK_a of HCOOH was found to be 19.0, which is similar to the 19.6 determined from direct methods. A combination of both direct and isodesmic methods have been often used to determine the pK_a of various acids in organic solutions with an expected error of ~ 1 pK_a unit.[16] As such, we expect the pK_a of HCOOH in MeCN to be close to the average value of 19.3.

Synthesis of $[DBU–H]^+$ Based Ionic Liquids

[DBU–H]PF_6. An aqueous solution (100 mL H_2O) of $[NH_4]PF_6$ (20.12 g, 123 mmol) was added to neat DBU (15.65 g, 103 mmol) with stirring. Upon addition of $[NH_4]PF_6$ a white solid precipitated from solution. After stirring the reaction mixture for 4 h the white solid was isolated by vacuum filtration, sequentially washed with H_2O (3 x ~15 mL) and hexanes (3 x ~15 mL), and dried in vacuo to give an off-white solid (22.62 g, 74%). ^{1}H NMR ($CDCl_3$, 600 MHz): δ_H 7.43 (br s, 1H, N*H*), 3.58-3.53 (m, 4H), 3.45 (br s, 2H), 2.68 (m, 2H), 2.09 (m, 2H), 1.78-1.72 (m, 6H). $^{13}C\{^1H\}$ NMR ($CDCl_3$, 600 MHz) δ_C 19.4, 23.7, 26.6, 29.0, 33.7, 38.8, 48.9, 55.1, 166.7. HR-LIFDI-MS $[M]^+$ *m/z*: calcd. for $C_9H_{17}N_2$, 153.1386; found, 153.1380.

[DBU–Et]PF_6. An aqueous solution (50 mL H_2O) of $[NH_4]PF_6$ (12.78 g, 78 mmol) was added to a stirring solution (50 mL of H_2O) of [DBU–Et]Br (17.07 g, 65 mmol). Upon addition of $[NH_4]PF_6$ a white solid precipitated from solution. After stirring the reaction

mixture for 4 h the white solid was isolated by vacuum filtration, sequentially washed with H_2O (3 x ~15) and hexanes (3 x ~15 mL), and dried in vacuo to give an off-white solid (19.7 g, 92 %). ^{1}H NMR ($CDCl_3$, 600 MHz): δ_H 3.64 (m, 2H), 3.57-3.49 (m, 6H), 2.82 (m, 2H), 2.12 (m, 2H), 1.79 (m, 6H), 1.27 (t, 3H). $^{13}C\{^1H\}$ NMR ($CDCl_3$, 600 MHz) δ_C 13.6, 20.1, 23.0, 26.2, 28.3, 28.8, 46.4, 49.1, 49.2, 55.4, 166.5. HR-LIFDI-MS $[M]^+$ *m/z*: calcd. for $C_{11}H_{21}N_2$, 181.1699; found, 181.1692.

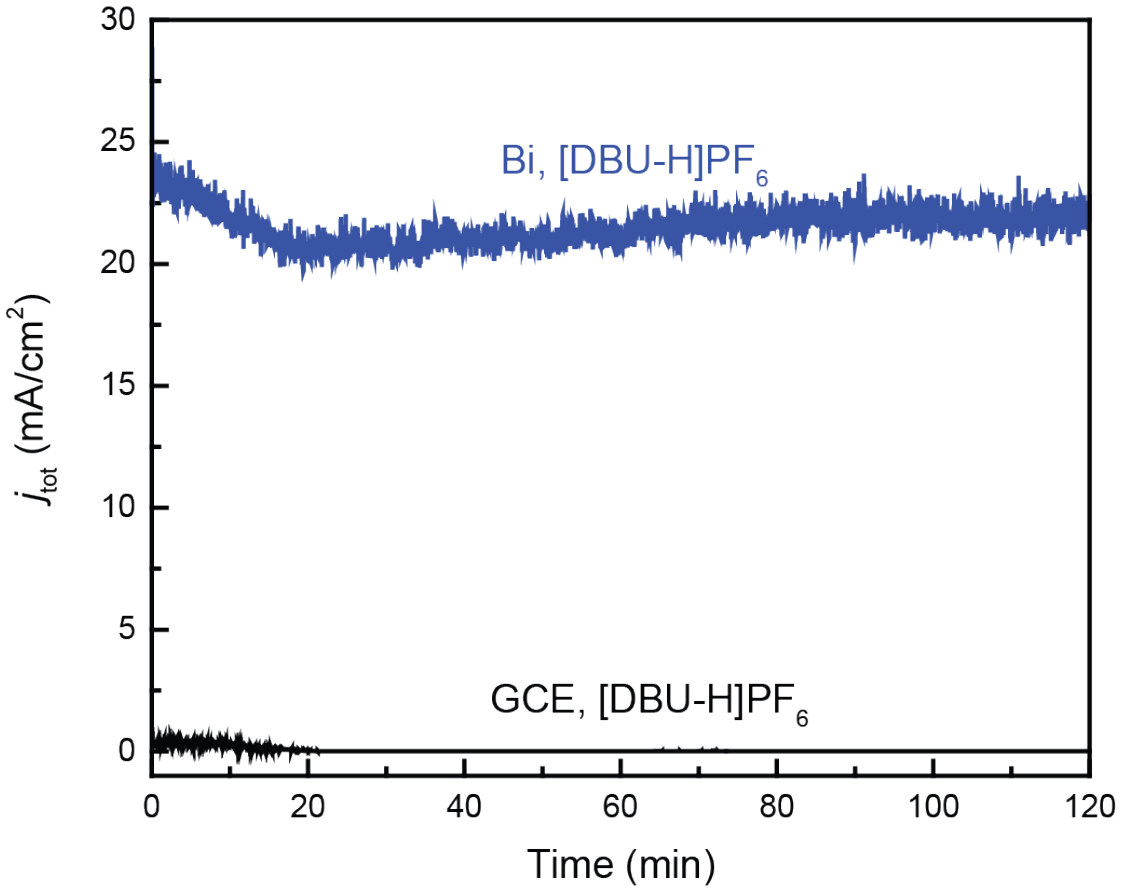

Figure S1. Total current density profiles recorded for Bi-electrodes (blue) and bare GCE (black) in CO_2 saturated MeCN solutions of 0.25 M [DBU-H]PF_6 at –1.80 V vs. SCE.

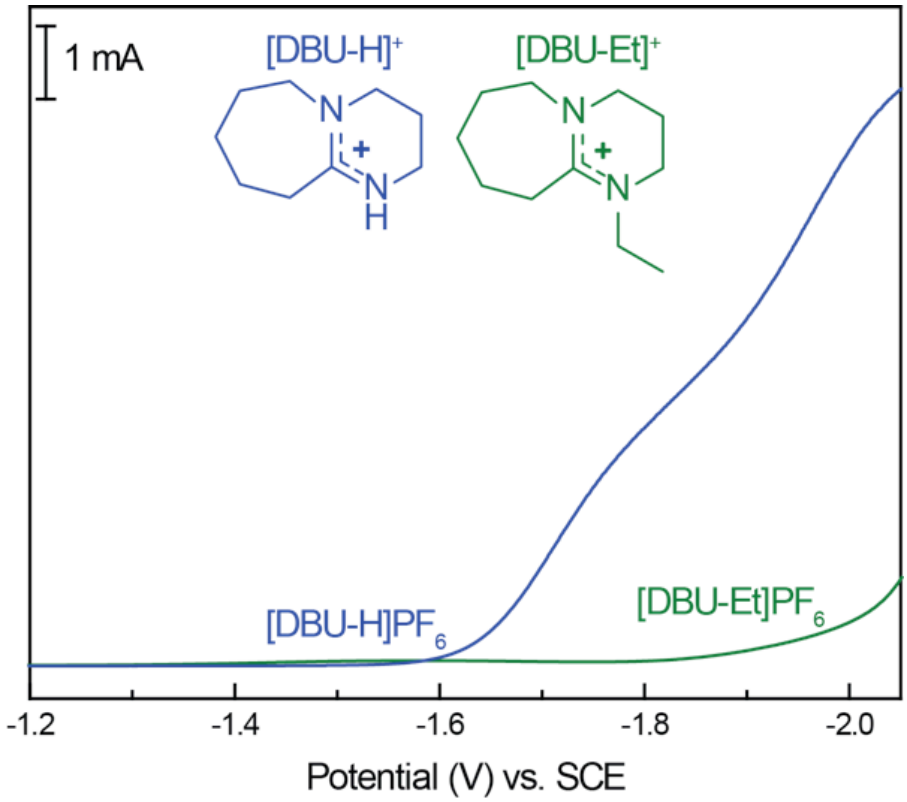

Figure S2. Linear sweep voltammograms (LSVs) recorded for a Bi-modified GCE in MeCN containing 0.1 M $TBAPF_6$ and 250 mM of either $[DBU–H]PF_6$ or $[DBU–Et]PF_6$.

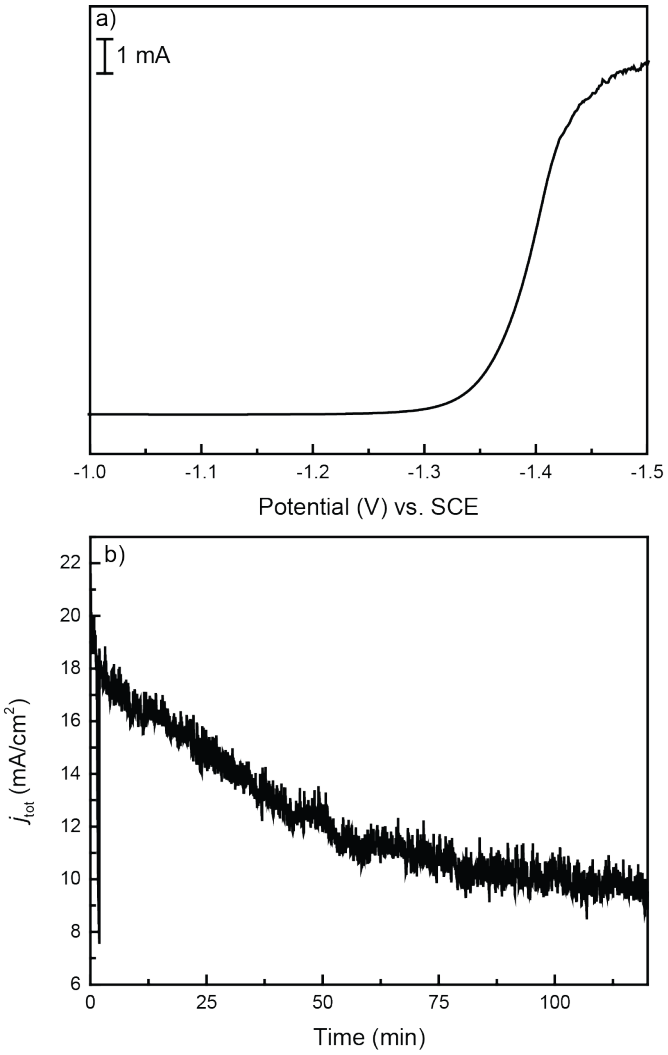

Figure S3. (a) LSV recorded for a Bi-modified GCE suspended in 0.5 M $NaHCO_3$ (pH 7.2) containing 100 mM [DBU–H]HCO_3; (b) total current density (j_{tot}) profile recorded for a Bi-modified GCE in 0.5 M $NaHCO_3$ containing 100 mM M [DBU–H]HCO_3 at E = –1.45 V vs. SCE.

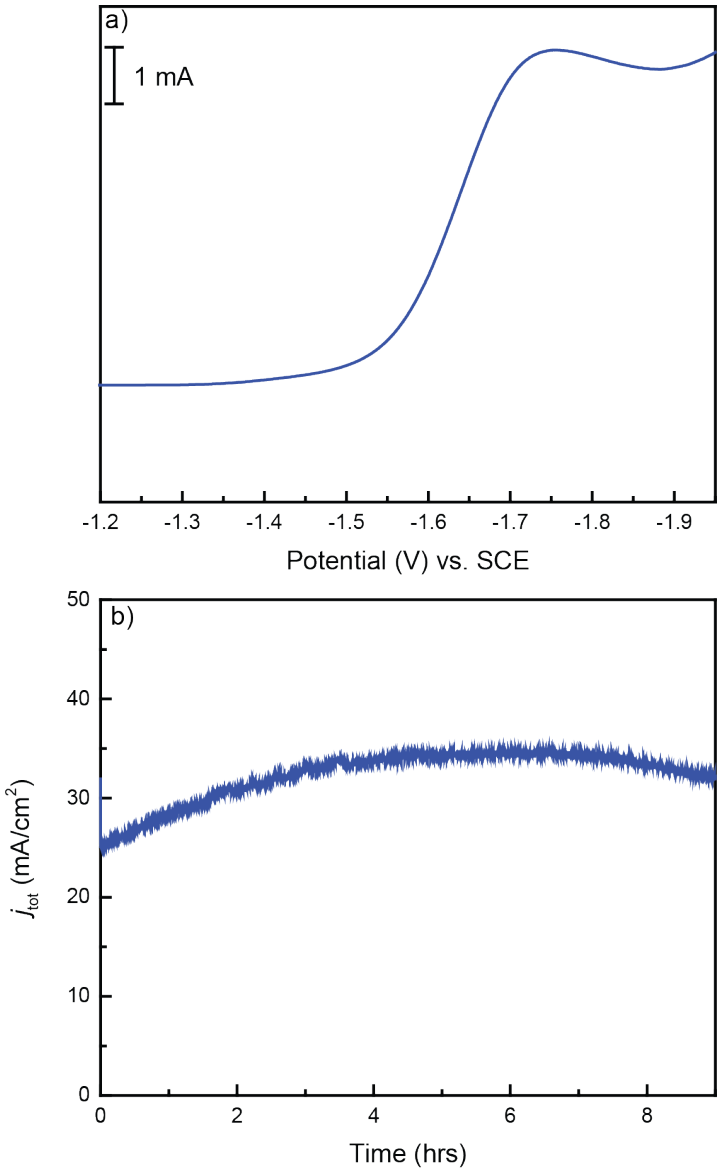

Figure S4. (a) CV trace recorded for Bi-modified GCE in CO_2–saturated MeCN/H_2O (95:5) containing 100 mM $TBAPF_6$ and 250 mM [DBU–H]PF_6 using a split solvent arrangement in which the anode compartment contained phosphate buffered water (pH 7.4); (b) total current density (j_{tot}) profiles recorded for Bi-modified GCE at E = –1.80 V under the same split solvent electrolysis conditions described in (a).

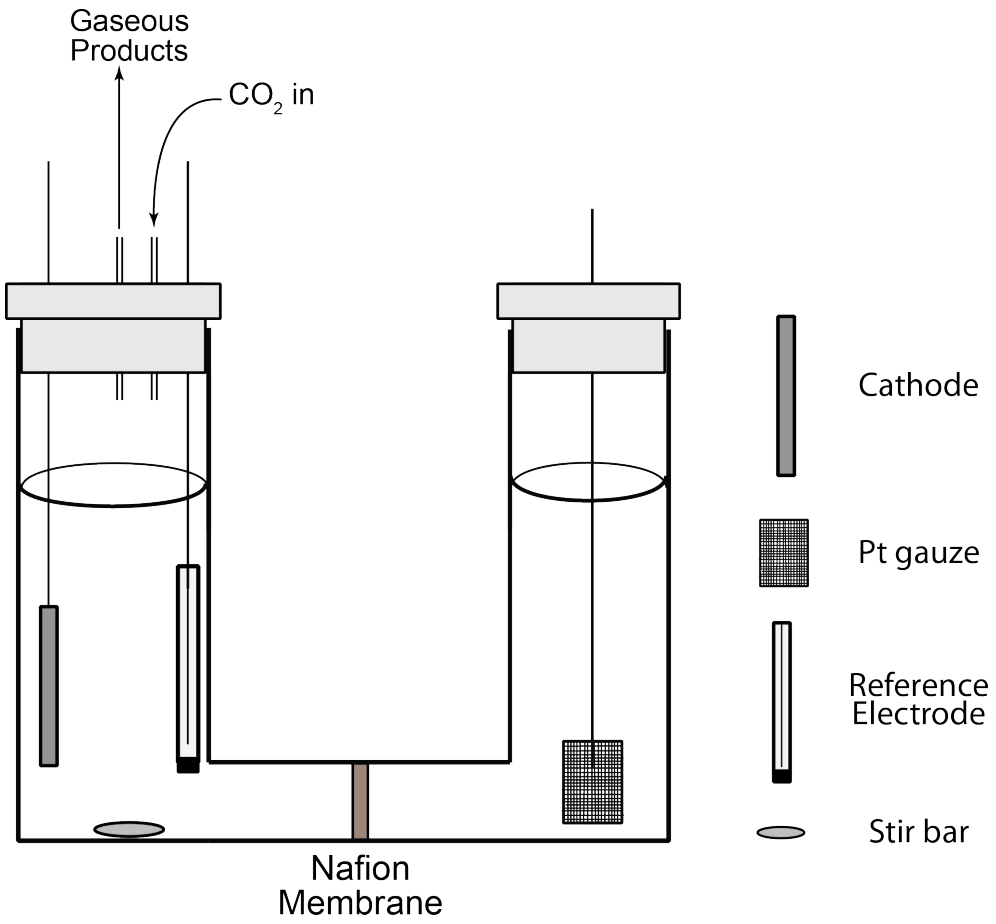

Figure S5. Schematic illustration of a two-compartment electrolysis cell employed for CO_2 electrolysis experiments.

(a)

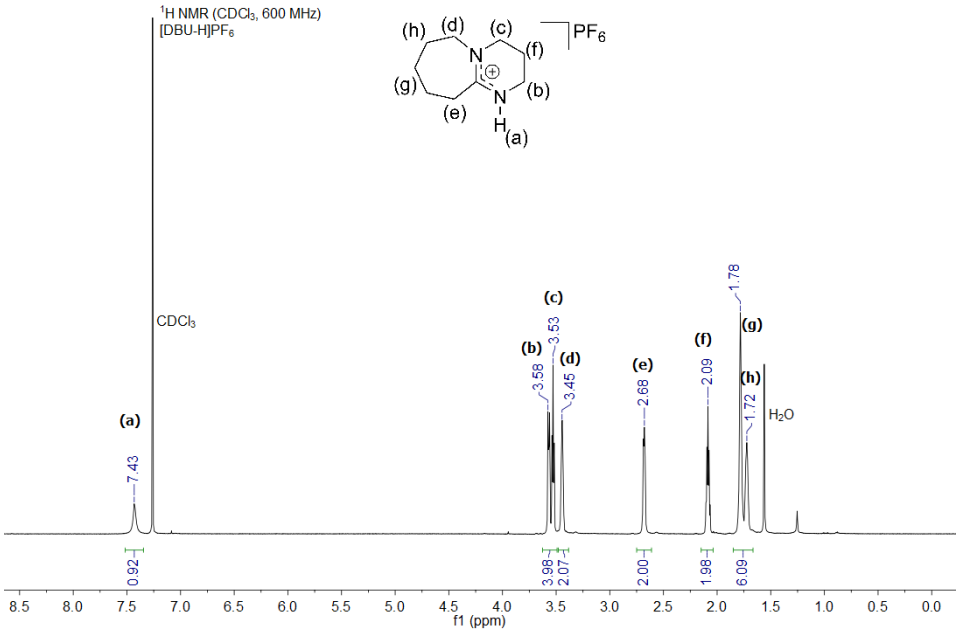

(b)

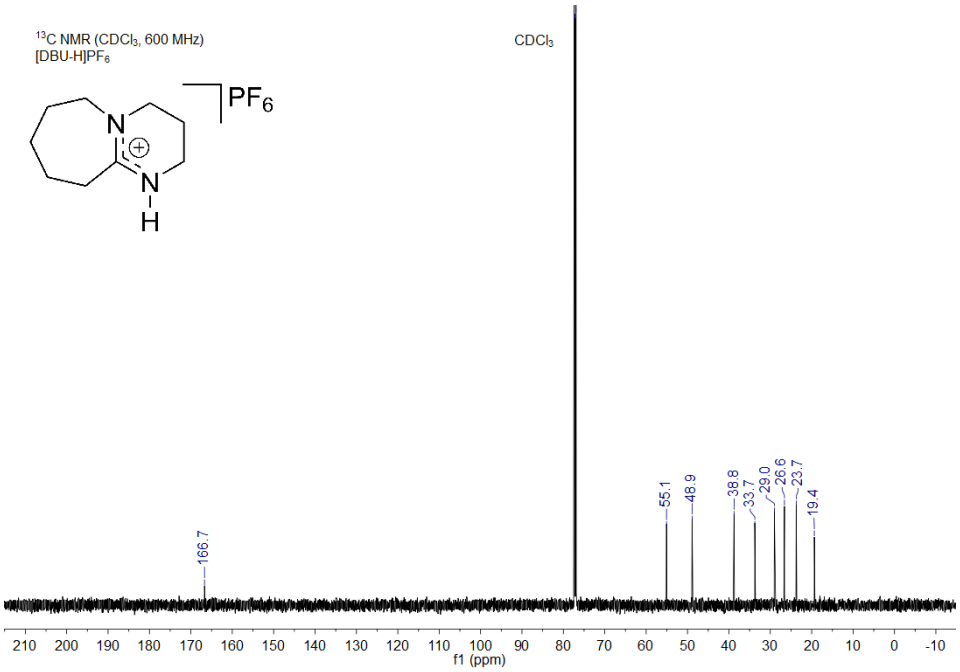

Figure S6. (a) ^{1}H and (b) ^{13}C NMR spectra recorded for [DBU–H]PF$_6$ in CDCl$_3$.

(a)

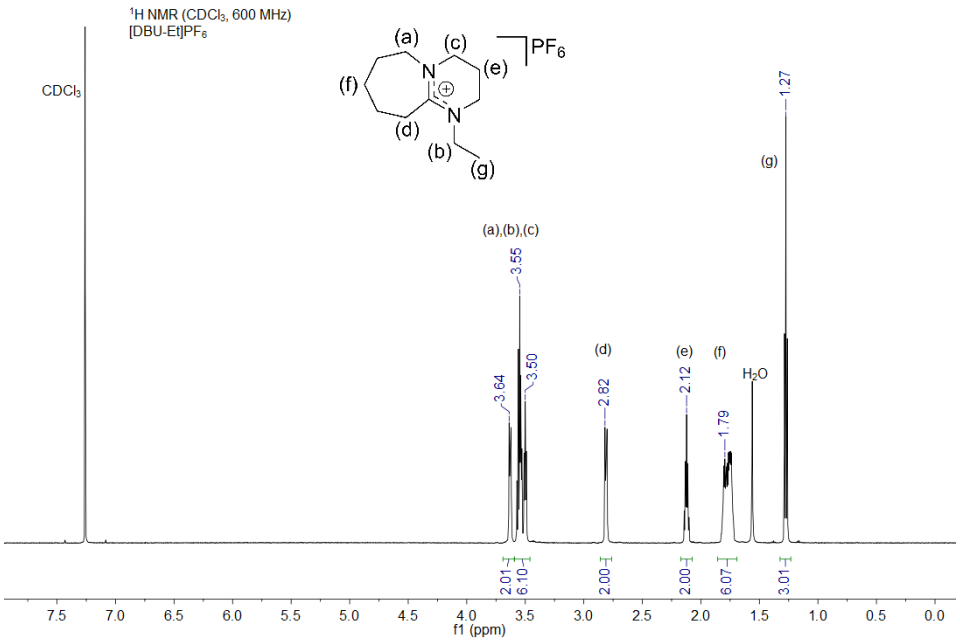

(b)

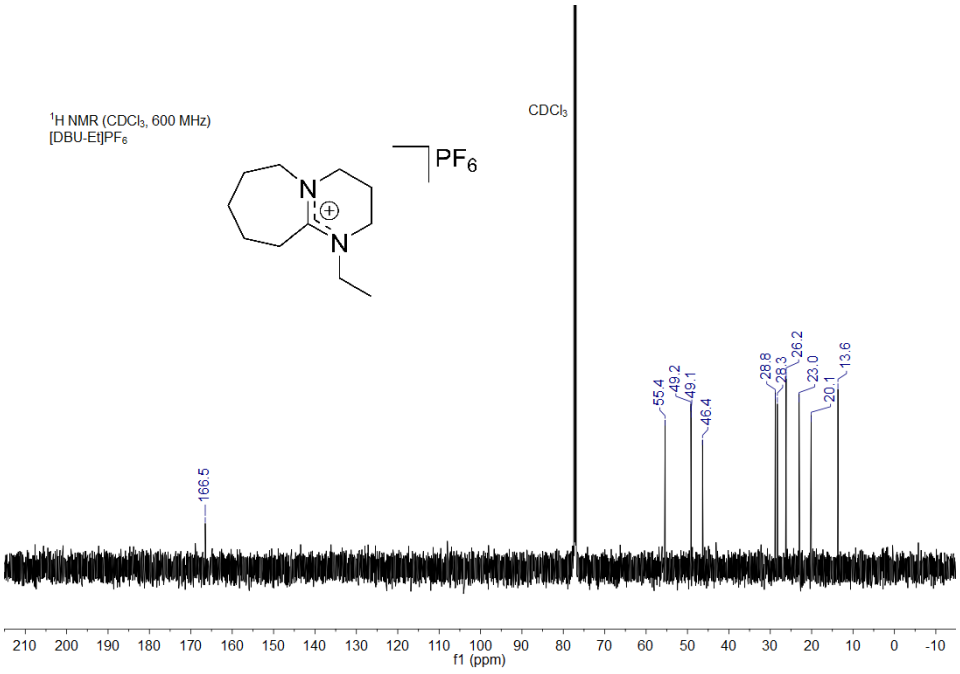

Figure S7. (a) ^{1}H and (b) ^{13}C NMR spectra recorded for [DBU–Et]PF_6 in $CDCl_3$.

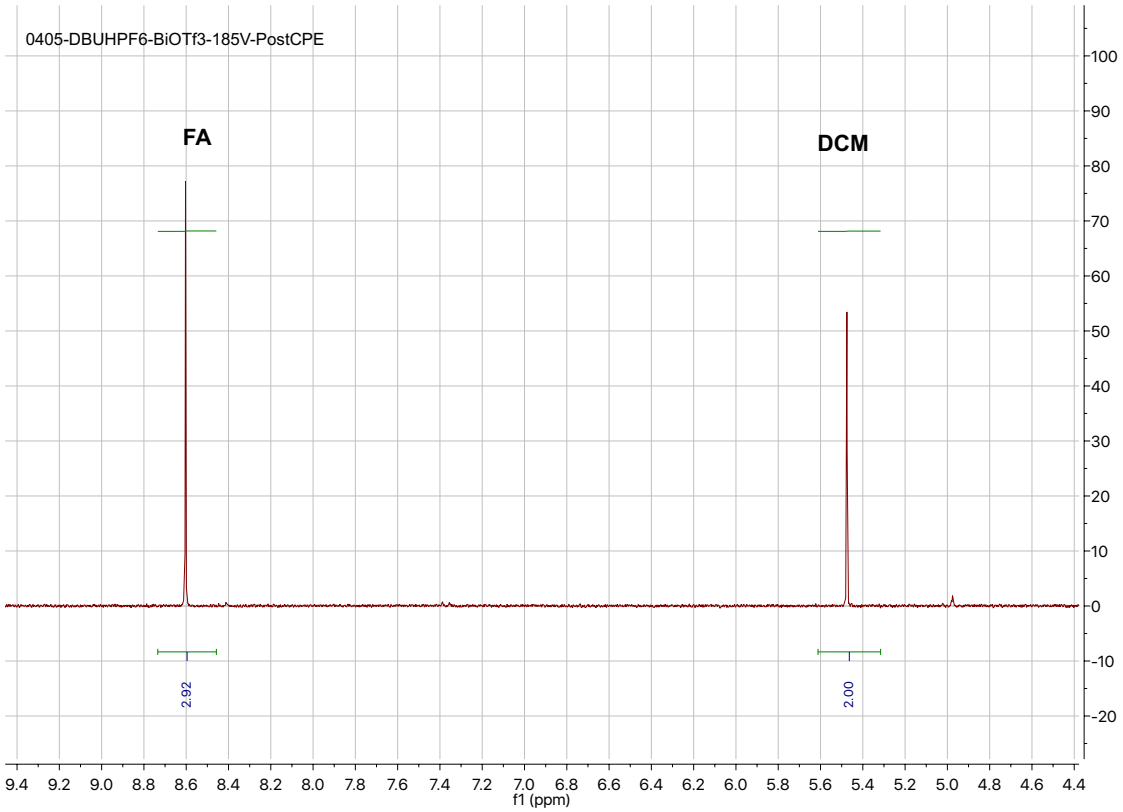

Figure S8. ^{1}H NMR spectrum of the post catholyte solution electrolyzed at –1.85V vs SCE, showing the integration of both the formate/formic acid (8.61 ppm) generated during electrolysis and the signal from the internal CH_2Cl_2 standard at 5.43 ppm.

1) DiMeglio, J. L.; Rosenthal, J., *J. Am. Chem. Soc*. **2013**, *135*, 8798.
2) Lethesh, K. C.; Shah, S. N.; Abdul Mutalib, M. I., *J. Chem. Eng. Data* **2014**, *59*, 1788.
3) Frisch, M. J.; Trucks, G. W.; Schlegel, H. B.; Scuseria, G. E.; Robb, M. A.; Cheeseman, J. R.; Scalmani, G.; Barone, V.; Mennucci, B.; Petersson, G. A.; et al. Gaussian 09, revision A.1; Gaussian, Inc.: Wallingford, CT, 2009.
4) Zhao, Y.; Truhlar, D. G. *Theor. Chem. Acc.* **2008**, *120*, 215.
5) Marenich, A. V.; Cramer, C. J.; Truhlar, D. G. *J. Phys. Chem. B* **2009**, *113*, 6378.
6) Price, W. S. *Annual Report NMR Spectroscopy* **1999**, *38*, 289.
7) Costentin, C.; Drouet, S.; Robert, M.; Savéant, J.-M. *Science* **2012**, *338*, 90.
8) Matsubara, Y.; Grills, D. C.; Kuwahara, Y. *ACS Catal*. **2015**, *5*, 6440.
9) Pegis, M. L.; Roberts, J. A. S.; Wasylenko, D. J.; Mader, E. A.; Appel, A. M.; Mayer, J. M. *Inorg. Chem*. **2015**, *54*, 11883.
10) CRC Handbook of Chemistry and Physics 96th edition, 2105–2016.
11) The value of ΔG_{vap} at 298K of formic acid was obtained from application of the Gibbs-Helmholtz equation to the ΔH_{vap} of formic acid listed in reference 10.
12) Roberts, J. A. S.; Bullock, R. M. *Inorg. Chem*. **2013**, *52*, 3823.
13) Connelly, N. G.; Geiger, W. E. *Chem. Rev.* **1996**, *96*, 877.
14) Shalev, H.; Evans, D. H. *J. Am. Chem. Soc.* **1989**, *111*, 2667.
15) Kaljurand, I.; Kütt, A.; Sooväli, L.; Rodima, T.; Mäemets, V.; Leito, I.; Koppel, I. A. J. Org. Chem. 2005, 70, 1019.
16) Ho, J.; Coote, M. L. *Theor. Chem. Acc.* **2009**, *125*, 3.
17) Moser, A.; Range, K.; York, D. M. *J. Phys. Chem. B* **2010**, *114*, 13911.
18) Kelly, C. P.; Cramer, C. J.; Truhlar, D. G. *J. Phys. Chem. B* **2007**, *111*, 408.
19) This values includes a standard state correction of 1.89 kcal/mol to correct for the difference between the gaseous standard state of 1 atm and the solution standard state of 1M
20) Izutsu, K. Acid-Base Dissociation Constants in Dipolar Aprotic Solvents; Blackwell Science, 1990.
21) Muckerman, J. T.; Skone, J. H.; Ning, M.; Wasada-Tsutsui, Y. *Biochim. Biophys. Acta* **2013**, *1827*, 882.
22) Keith, J. A.; Grice, K. A.; Kubiak, C. P.; Carter, E. A. *J. Am. Chem. Soc.* **2013**, *135*, 15823.